Intermolecular Spin-Spin Coupling in Highly Fluorinated Solutions of Galvinoxyl Free Radical

Huseyin Ovalioglu, Ahmet Peksoz, Handan Engin Kirimli, and Aytac Yalciner

Physics Department, Sciences and Arts Faculty, Uludag University, Gorukle Campus, 16059, Bursa, Turkey

Reprint requests to Prof. Dr. A. Y.; Fax: +90 224 29 41 899; E-mail: aytac@uludag.edu.tr

Z. Naturforsch. **65a,** 254 – 262 (2010); received February 20, 2009 / revised July 16, 2009

Overhauser effect type dynamic nuclear polarization experiments were performed to study the solutions of the stable free radical Galvinoxyl in highly fluorinated aliphatic and aromatic solvents. Mainly the Overhauser effect, which normally arises due to both dipolar and scalar interactions between the unpaired electrons of the free radical molecules and fluorine nuclei of solvent molecules, occurs here in the solutions, which are examined in this study. As solvent, N-methyl-bistrifluoroacetamide and octafluorotoluene were used. The experiments were performed at a low field double resonance nuclear magnetic resonance (NMR) spectrometer, which operates at 1.53 mT. The NMR enhancements depend on competition between intermolecular magnetic interactions. We investigated the NMR enhancement factors depending on the electron spin resonance (ESR) frequency, which is modulated by the interaction between the electron spin of the free radical and the nuclear spins in its vicinity, at four different temperatures. It was found that the electron spin of the free radical interact very strongly with the nitrogen atom of the N-methyl-bistrifluoroacetamide molecule rather than hydrogen atoms of own radical molecule. Galvinoxyl free radical doesn't show this interaction with the other solvents at the weak field. This effect, which has been reported as an intramolecular interaction previously, is observed for the first time as an intermolecular coupling in this study.

Key words: Dynamic Nuclear Polarization; Overhauser Effect; Fluorine-Electron Double Resonance; Free Radical; ESR Spectra.

1. Introduction

Dynamic nuclear polarization (DNP) is a well-known double resonance technique of the magnetic resonance. In this technique, the nuclear magnetic resonance (NMR) signal is observed simultaneously with the irradiation of the electron spin resonance (ESR). In the Overhauser effect (OE) type DNP for free radical solutions, when the ESR of the paramagnetic solute is saturated, important changes in the intensity of the NMR signal of the solvent occur [1, 2]. The positive or negative DNP enhancements can be observed depending on whether the scalar or the dipolar coupling is dominant.

The studies at the low magnetic fields are of importance in order to obtain comparable interaction parameters for the various systems. DNP is sensitive to variations of the ratio of the dipolar and the scalar couplings. The dipolar interactions depend on the geometrical structures of the colliding molecules. The scalar interactions depend on the chemical environment of both receptor nucleus and unpaired electron.

Yalçıner [3] investigated the ESR hyperfine structure of α,γ-bisdiphenylene-β-phenyl allyl free radical in solutions of toluene and benzene against different concentration via Overhauser effect in weak fields. The α,γ-bisdiphenylene-β-phenyl allyl free radical has fourteen mesomeric aspects. It was reported that the ESR spectra should not be affected by the solvents under the condition that there is no association between the solvent and free radical molecules, since the transitions are due to the couplings of the unpaired electron of the free radical molecule with its nearest own protons. Müller-Warmuth [4] investigated potassium nitrosodisulfonate radical ions $(SO_3)_2NO^-$ in water, in which the interaction between the electron and the nitrogen is intramolecular. Sünnetçioğlu et al. [5] investigated hyperfine structure and relaxation times of 4-Oxo-TEMPO/methyl alcohol solutions in weak and strong fields, in which the interaction between the unpaired electron located on the oxygen atom and nitrogen atom is intramolecular. Salman et al. [6] investigated π and σ transitions for nitroxide

spin probes 4-hydroxy-TEMPO and 4-amino-TEMPO at 1.53 mT, in which the interaction between the unpaired electron and the nitrogen atom is intramolecular. Sert et al. [7] studied the dynamic nuclear polarization of 4-hydroxy-TEMPO/water-glycerol solutions in weak fields, in which the interaction between the unpaired electron and the nitrogen atom is intramolecular.

Recently, DNP technique in the intermolecular spin-spin interactions in liquid samples has also been applied in the low magnetic field studies of biological liquids, free radical imaging, oximetry, and char suspensions, by Grucker et al. [8, 9], De Sousa et al. [10], Planinšič et al. [11], Clarkson et al. [12], and Peksoz et al. [13]. In particular, Clarkson et al. [12] observed that the dipole-dipole interaction and the scalar interaction between the protons in water and the free electrons in char are dominant separately. Mülsch et al. [14], Nestle et al. [15], and Lurie et al. [16] studied proton-electron double resonance imaging (PEDRI). Kleschyov et al. [17] have worked an electron paramagnetic spin trapping of biological nitric oxide and reported that the number of biomedical applications of EPR is constantly increasing.

The NMR enhancements depend on the competition between the dipolar and the scalar contact part of the coupling, between solvent nuclei and radical's unpaired electron. The aim of this work is to investigate the NMR signal during simultaneous irradiation of the ESR for the solutions of Galvinoxyl (GALV) free radical in two highly fluorinated aliphatic and aromatic solvents in a low magnetic field of 1.53 mT for four different temperatures, and thus to determine the form and peak points, i. e. the transition frequencies of the ESR spectra depending on the temperature. The ESR hyperfine structure of GALV in solutions of N-methyl-bis-trifluoroacetamide (MBFA) and octafluorotoluene (OFT) was investigated for the first time in this work and observed an effect which has not been reported previously. It was found that the spectra for the GALV/MBFA solutions can be interpreted simply as the unpaired electron spin of the free radical molecule interacting with the nitrogen atom of the solvent molecule very strongly.

2. Theory

The full theory of the OE, in low magnetic fields, has been given previously [18 – 20]. Here the theory will be reviewed shortly. Figure 1 shows the energy level diagram of a nucleus with spin 1/2 and an electron

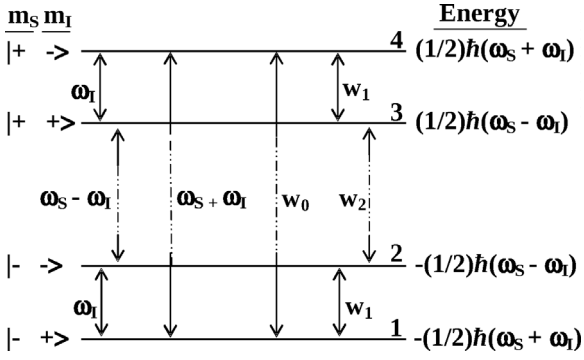

Fig. 1. Energy level diagram of a nucleus with a 1/2 spin and an electron two-spin system. m_S and m_I are the magnetic quantum numbers for electron and nucleus, respectively. w_i (i = 0, 1, 2), ω_S and ω_I are the transition probabilities and the transition frequencies, respectively. Energies are given for each level. $\omega_S/\omega_I = 700$; the transitions in the figure are shown as dotted-dashed lines.

two-spin system. m_S and m_I are the magnetic quantum numbers for electron and nucleus, respectively. For this system, the transition probabilities via relaxation w_0, w_1, and w_2 can be given as

	$m_S m_I$	$m_S m_I$	
w_0	$\|+-\rangle \Leftrightarrow \|-+\rangle$	flip-flop (with the frequency $\omega_S + \omega_I$)
w_2	$\|++\rangle \Leftrightarrow \|--\rangle$	flip-flop (with the frequency $\omega_S - \omega_I$)
w_1	$\|\pm-\rangle \Leftrightarrow \|\pm+\rangle$	m_S= constant (with the frequency ω_I)

,

where $w_1 = w_1' + w_1''$. $2w_1'$ is the transition probability due to the nuclear-electron spin coupling and $2w_1''$ the transition probability due to the other relaxation mechanisms.

An expression for the equation of motion of the nuclear polarization can be written as [21]

$$\frac{dP_z}{dt} = -(w_0 + 2w_1 + w_2) \cdot \left[(P_z - P_0) - \frac{w_2 - w_0}{w_0 + 2w_1 + w_2} (\Pi_z - \Pi_0) \right], \quad (1)$$

where P_z and Π_z represent the dynamic polarization of nuclear spins and unpaired electron spins, respectively, and P_0 and Π_0 represent the polarizations at the thermal equilibrium.

In the steady state, i. e. $dP_z/dt = 0$, the Overhauser enhancement factor is defined as

$$A = \frac{P_z - P_0}{P_0} = \rho f s \left| \frac{\gamma_S}{\gamma_I} \right|, \quad (2)$$

where γ_S ($\gamma_S < 0$) and γ_I ($\gamma_I > 0$) are electronic and nuclear gyromagnetic ratios, respectively, f is the leakage

factor for the nuclear relaxation, s is the saturation factor which is equal to 1 for the complete ESR saturation ($0 \leq s \leq 1$), ρ is the nuclear-electron coupling parameter, which is a measure of the nature and the random time dependence of the nuclear-electron interaction.

2.1. Intramolecular Spin-Spin Coupling [3, 4]

Let us consider a free radical in a magnetic field. The unpaired electron of the radical molecule is represented by a wave function Ψ_m, where m is a magnetic quantum number. Electron polarization can be written as

$$\Pi_Z = -\frac{1}{S}\sum_m \langle m|S_z|m\rangle \frac{N_m}{N}, \tag{3}$$

where S_z is the z-component of the spin operator S (S_x, S_y, S_z), and N_m is the population in the Ψ_m state. The summation includes all the states. A magnetic field with the frequency ω,

$$H_x = 2H_{1e}\cos\omega t \tag{4}$$

can excite the magnetic dipolar transition which has a resonance frequency near to ω. Consequently, the electron polarization Π_z is exceedingly affected by this transition. The probability of absorption or emission per unit time can be calculated with the perturbation theory as

$$W_{ik} = 2\pi\gamma_s^2 H_{1e}^2 g(\omega-\omega_{ik})\left|\langle m_i|S_x|m_k\rangle\right|^2. \tag{5}$$

The shape function $g(\omega-\omega_{ik})$ is normalized as

$$\int_{-\infty}^{\infty} g(\omega-\omega_{ik})\mathrm{d}\omega = 1, \tag{6}$$

and has a maximum for $\omega = \omega_{ik}$,

$$g(0) = T_2^{ik}/\pi \tag{7}$$

(this is also the definition of the transversal relaxation time T_2^{ik}).

The change in population for any state m is given by

$$\frac{\mathrm{d}N_m}{\mathrm{d}t} = \sum_{n\neq m}\left[-N_m(w_{mn}+W_{mn})+N_n(w_{nm}+W_{nm})\right], \tag{8}$$

where $W_{nm} = W_{mn}$ is given by (5), and w_{nm} and w_{mn} are the relaxation transition probabilities due to the spin-lattice coupling. They satisfy the Boltzmann distribution

$$\frac{w_{nm}}{w_{mn}} = \exp\left[\frac{\hbar\omega_{nm}}{kT}\right]. \tag{9}$$

2.2. Inhomogenous Broadening of ESR-Lines [3, 4, 7]

In most cases the appearance of the hyperfine structure spectra is so ambiguous that it is very hard to distinguish the separate components. In this case the parameter s of the electron spin system can be given by

$$s = \int_{-\infty}^{\infty} \frac{\sigma_{ik} g(\omega-\omega_{ik})}{1+\sigma_{ik} g(\omega-\omega_{ik})} h(\omega_{ik})\mathrm{d}\omega_{ik}, \tag{10}$$

where

$$\int_{-\infty}^{\infty} h(\omega_{ik})\mathrm{d}\omega_{ik} = 1. \tag{11}$$

Dynamic nuclear polarization and ESR parameters are related in the following two cases for which the integral (10) can be easily calculated [3]:

(i) The inhomogeneous line broadening is larger than the line width of a single ESR-line.

(ii) The local field distribution has a Lorentz form.

In the former $\mathbf{H}_{1e}$ must not be too large, otherwise the broadening due to saturation invalidates the condition. On the other hand, for only $\omega \approx \omega_{ik}$ $g(\omega-\omega_{ik}) \neq 0$, $h(\omega_{ik})$ is approximately constant in this region. When $g(\omega-\omega_{ik})$ acquires Lorentz form, it can be written as

$$g(\omega-\omega_{ik}) = \frac{T_{2e}^{ik}}{\pi}\frac{1}{1+(\omega-\omega_{ik})^2(T_{2e}^{ik})^2}, \tag{12}$$

and all the T_{1e}^{ik} and T_{2e}^{ik} are equal in this frequency interval within the range of the experimental errors. From (10), one can obtain

$$s = h(\omega)\frac{\sigma T_{2e}}{\pi}\int_{-\infty}^{\infty}\frac{\mathrm{d}\omega_{ik}}{1+(\omega-\omega_{ik})T_{2e}^2+(\sigma/\pi)T_{2e}}, \tag{13}$$

or

$$s = \frac{\sigma h(\omega)}{\sqrt{1+(\sigma/\pi)T_{2e}}} \tag{14}$$

in the second case

$$h(\omega_{ik}-\omega_0) = \frac{T_{2e}^*}{\pi}\frac{1}{1+(\omega_{ik}-\omega_0)^2+T_{2e}^{*\,2}}. \tag{15}$$

If g has a Lorentz form and T_{1e}^{ik} and T_{2e}^{ik} satisfy the above condition, the integration of (10) gives

$$s = \frac{\sigma/\pi}{\sqrt{1+(\sigma/\pi)T_2}}\frac{\tau}{1+(\omega-\omega_0)^2\tau^2}, \tag{16}$$

where

$$\frac{1}{\tau} = \frac{1}{T_{2e}^*} + \frac{1}{T_{2e}}\sqrt{1+(\sigma/\pi)T_{2e}}\,. \tag{17}$$

Under the condition $(\sigma/\pi)T_{2e} \ll 1$ the measurements of P_z/P_0 for various ESR frequencies ω gives in the first case $h(\omega)$ and in the second case the line broadening parameter of the total Lorentz curve $\tau(H_{1e})$.

2.3. Energy Levels and Magnetic Dipole Transitions

The Hamiltonian of the nitrogen-electron system can be given by [4, 5]

$$\begin{aligned}\mathcal{H} &= \hbar\gamma_s B_0 S_z + A_1 S_z I_{NZ} + A_2 S_z I_{NZ} \\ &+ \frac{A_1}{2}\{S^+ I_N^- + S^- I_N^+\} + \frac{A_2}{2}\{S^+ I_N^- + S^- I_N^+\}\end{aligned} \tag{18}$$

for two different complex formation, i. e. for two different hyperfine coupling constants A_1 and A_2, when taking into consideration that $\gamma_s \gg \gamma_{IN}$ for the gyromagnetic ratios.

The high-resolution energy levels of the system can be calculated from the well-known Breit-Rabi formula [4],

$$E_m = -\frac{\delta W_i}{6} \mp \frac{\delta W_i}{2}\sqrt{1+x_i{}^2+\frac{4}{3}m_F x_i}, \quad (i=1,2), \tag{19}$$

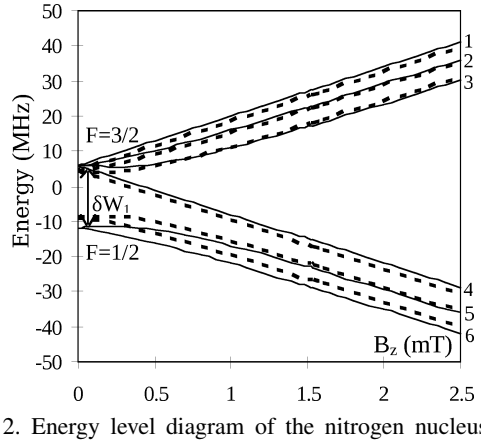

Fig. 2. Energy level diagram of the nitrogen nucleus-free electron system for two different hyperfine coupling constants A_1 (—) and A_2 (---) according to the Breit-Rabi equation. The energy levels 1 – 4 for $F = 3/2$ and 5 – 6 for $F = 1/2$ are shown in MHz versus the magnetic field in mT. δw_1 is the zero field splitting for A_1.

where $\delta W_i = \frac{3}{2}A_i$ is the hyperfine splitting and $x_i = \frac{\gamma_s \hbar B_0}{\delta W_i}$. The + sign valids for the levels 1 – 4, the − sign for level 5 and 6. In Figure 2 the energy levels are shown in MHz versus the low and medium magnetic fields, in which the levels are labeled as 1 to 6. The selection rules permit the magnetic dipole transitions if $\Delta m = \pm 1$ (π-transition) 1-2, 1-6, 2-3, 2-5, 3-4, 3-6, 4-5, and 5-6, and $\Delta m = 0$ (σ-transition) 2-6 and 3-5.

The transition probabilities can easily be calculated for each transition using an usual calculation method.

3. Experimental

The stable free radical GALV and the solvents used in this study were taken from Aldrich Chem. Co. (USA), and Fluka (Switzerland), respectively. The purities of the solvents are 97 % and 98 %. The solvents are N-methyl-bis-trifluoroacetamide (MBFA) (Fig. 3), and Octafluorotoluene (OFT). To prepare the samples, GALV was firstly weighted, dissolved in solvent (3.0 mM), and the samples in pyrex tubes of 18 mm diameter were degassed by using at least five freeze-pump-thaw cycles with liquid nitrogen at about 10^{-3} Pa in the Leybold-Heraeus vacuum system and were then sealed. The degassing procedure is necessary, because otherwise the oxygen in the sample

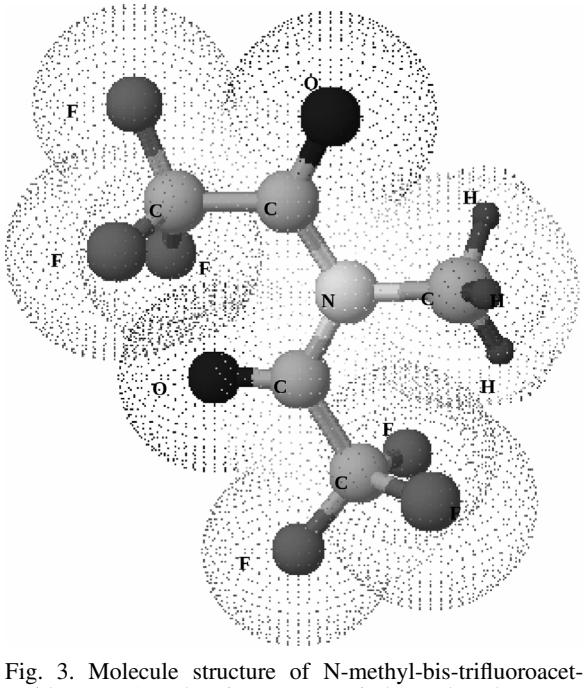

Fig. 3. Molecule structure of N-methyl-bis-trifluoroacetamide (MBFA). The nitrogen atom is located at the centre of the molecule.

would not permit easy stimulation of the electron spin resonance (ESR) lines.

The experiments were performed at a low field double resonance NMR spectrometer, which operates at 1.53 mT [22]. The spectrometer which uses the continuous-wave technique has a resonance frequency of 61.2 kHz for ^{19}F nuclei and 43 MHz for electrons. The signals are detected by the amplitude modulation technique, using Q-meter detection, and then they are amplified in a low frequency, narrow-band amplifier, which is connected to a phase sensitive detector and then to a recorder. The external magnetic field is swept by a digital sweep generator [22]. The spectrometer has also an automatic temperature control system using the liquid nitrogen vapor or heated air flow [23, 24].

In the low field DNP investigations, the observations are based on the pure and the double resonance NMR signal intensities (P_0 and P_z). The usual amplitude modulation technique gives the signals as the derivatives of the central bands, first and second side bands. The P_0 and P_z values were taken as the peak-to-peak values of the derivatives of the central bands.

The experiments for each sample were performed in the liquid phase with an accuracy of ± 2 °C. For each sample, in four different temperatures, P_0 was measured four times and P_z values were obtained depending on the ESR frequency. The enhanced signal P_z should not be saturated; to satisfy this condition, the ESR voltage V_{eff} (V)/ESR frequency f (MHz) ratio was kept as 1/2 over the frequency range. So the enhancement factor $(P_z - P_0)/P_0$ is obtained for each ESR frequency. The r. f. signal in the 25 – 65 MHz frequency range for the ESR coil were taken from the Rohde & Schwarz sml 01 signal generator, amplified with a T&C Power Conversion LA-50 HF amplifier, and measured with an electronic HF voltmeter Anritsu ML 69A.

4. Results and Discussion

Figure 4 shows the GALV/MBFA spectrum obtained at the 31 – 59 MHz frequency range at four different temperatures. Figure 5 shows the GALV/OFT spectrum obtained at the 31 – 61 MHz frequency range at four different temperatures.

At the peak points of ESR spectra, the enhancement factor $-(P_z - P_0)/P_0$ increases as the temperature decreases.

The GALV/OFT spectrum is simply a superposition of some Lorentzians corresponding to the transitions of intramolecular spin-spin interaction in GALV.

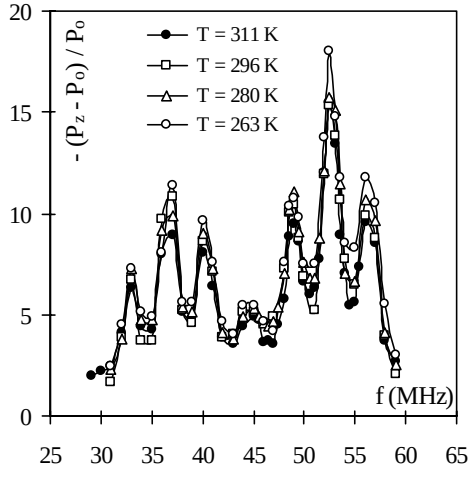

Fig. 4. ESR spectra of the GALV/MBFA sample for four different temperatures. The variation of the enhancement factor $-[(P_z - P_0)/P_0]$ with the ESR frequency f (MHz) is given for the temperatures ○ 263 K, △ 280 K, □ 296 K, and • 311 K. Experimental points and the fit function which is the sum of seven Gaussians (20) are shown.

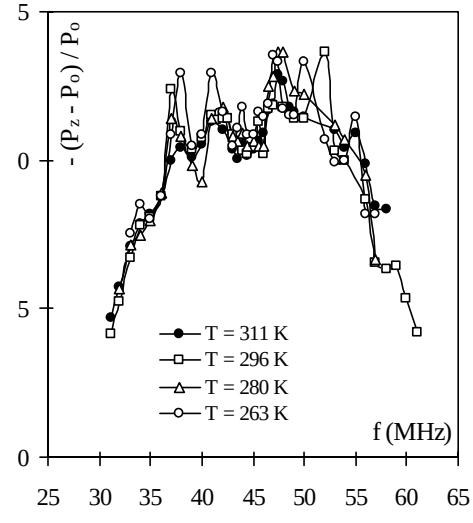

Fig. 5. ESR spectra of the GALV/OFT sample for four different temperatures. The variation of the enhancement factor $-[(P_z - P_0)/P_0]$ with the ESR frequency f (MHz) is given for the temperatures ○ 263 K, △ 280 K, □ 296 K, and • 311 K. The curves are drawn to guide the eye.

To interpret the GALV/MBFA spectrum, we need much more lines than for the GALV/OFT. The experimental points can be fitted to a sum of seven Gaussians

$$y = \sum_{i=1}^{7} K_i \cdot \exp(-0.5 \cdot ((x - x_{ci})/w_i)^2), \qquad (20)$$

Table 1. The experimental points of the GALV/MBFA spectrum can be fitted to a sum of seven Gaussians given in (20). Fit parameters are tabulated for four temperatures.

		263 K	280 K	296 K	311 K
ESR Frequency at the Peak Point (MHz)	x_{c1}	33.16	32.99	32.90	33.09
	x_{c2}	36.81	36.61	36.63	36.79
	x_{c3}	40.18	40.22	40.20	40.20
	x_{c4}	44.58	44.69	44.75	44.67
	x_{c5}	49.02	49.13	49.02	49.15
	x_{c6}	52.51	52.66	52.62	52.57
	x_{c7}	56.31	56.38	56.32	56.37
Weight of the individual Gaussian	K_1	6.73	6.64	6.47	5.07
	K_2	11.20	10.53	11.68	8.01
	K_3	9.38	8.79	8.13	7.76
	K_4	5.61	5.33	5.21	4.96
	K_5	10.50	10.10	9.32	9.17
	K_6	16.42	15.15	14.80	14.49
	K_7	11.72	10.88	9.93	9.31
Standart Deviation of the individual Gaussian (MHz)	w_1	1.45	1.17	1.00	2.30
	w_2	0.88	1.04	1.00	0.89
	w_3	1.06	1.05	0.94	1.14
	w_4	1.87	1.87	2.36	1.72
	w_5	1.09	1.19	1.03	1.15
	w_6	0.97	0.94	0.96	0.90
	w_7	1.48	1.26	1.33	1.39

where $y = -(P_z - P_0)/P_0$, the K_i values are the enhancements at the peak points, the x_{ci}'s are ESR frequencies at the peak points, and the w_i's are the standard deviations of the individual Gaussians. All of the fit parameters are given for the temperatures of 263 K, 280 K, 296 K, and 311 K in Table 1. The R^2 values are 0.986, 0.981, 0.993, and 0.971, respectively, which point out the degree of agreement between the experimental fit function (20) and the experimental values.

The high resolution of the ESR spectrum arises in this case from the interaction of the unpaired electron spin, delocalized on the oxygen atom of the GALV free radical molecule, and the nitrogen nucleus localized at the centre of the MBFA molecule. Mukaı et al. [25] have investigated anomalous magnetic properties of crystalline GALV radical in tetrahydrofuran (THF) at room temperature using a JES-ME-3X spectrometer. They found a twin quintet hyperfine splitting, which is modulated by the interaction between the unpaired electron spin and the proton spins of GALV free radical molecule.

Table 3. Transition frequencies for four temperatures. The transitions of 2-5 and 3-6 are at the same frequencies.

Hyperfine coupling constant	Transition at 1.53 mT	Type		ESR Frequency at the Peak Point (MHz)
A_1	3-4	π	x_{c1}	32.7
	3-5	σ	x_{c2}	40.6
	2-5	π	x_{c3}	46.2
	3-6	π	x_{c4}	46.2
	2-6	σ	x_{c5}	51.8
	1-6	π	x_{c6}	56.3
A_2	3-4	π	x_{c7}	35.0
	3-5	σ	x_{c8}	40.4
	2-5	π	x_{c9}	44.7
	3-6	π	x_{c10}	44.7
	2-6	σ	x_{c11}	49.0
	1-6	π	x_{c12}	52.6

Table 4. Weight of the individual Gaussian K_i at four different temperatures.

Hyperfine coupling constant	Transition at 1.53 mT	Type		263 K	280 K	296 K	311 K
A_1	3-4	π	K_1	7.75	7.75	7.75	7.00
	3-5	σ	K_2	5.00	4.60	4.50	4.15
	2-5	π	K_3	1.70	1.50	1.50	1.50
	3-6	π	K_4	1.70	1.50	1.50	1.50
	2-6	σ	K_5	4.00	4.00	4.00	4.00
	1-6	π	K_6	12.00	11.00	10.20	10.00
A_2	3-4	π	K_7	11.25	9.75	11.00	9.00
	3-5	σ	K_8	5.00	4.60	4.50	4.15
	2-5	π	K_9	1.70	1.50	1.50	1.50
	3-6	π	K_{10}	1.70	1.50	1.50	1.50
	2-6	σ	K_{11}	10.50	10.25	9.90	9.15
	1-6	π	K_{12}	14.75	12.70	12.40	12.30

So far only the intramolecular Overhauser type spin-spin coupling in the free radical solutions was observed in weak field, and all of them could be explained with the well-known Breit-Rabi formula. The effect observed in this work was not reported previously. For this interaction the Hamiltonian of the nitrogen nucleus-free electron system for two different hyperfine coupling constants A_1 and A_2 had been given in (18). The Breit-Rabi formula, which gives energies depending on the magnetic field intensity, had been given in (19).

Table 2. All possible transition frequencies in MHz at 1.53 mT for the GALV/MBFA system. The observed transitions are 1-6, 2-5, 3-4, 3-6, 2-6, and 3-5. It were taken two different hyperfine coupling constants A_1 and A_2.

Transition type	π	π	π	π	π	π	π	π	σ	σ
Transition	1-2	2-3*	5-6*	4-5	3-4	2-5*	3-6*	1-6	3-5	2-6
A_1 = 12.01 MHz	4.57	5.58	5.58	7.87	32.73	46.17	46.17	56.32	40.60	51.75
A_2 = 8.92 MHz	3.63	4.28	4.28	5.47	34.97	44.71	44.71	52.62	40.44	48.99

* The transitions of 2-3 and 5-6, and 2-5 and 3-6 are at the same frequency.

Table 5. Standart Deviation of the individual Gaussian w_i (in MHz) at four different temperatures.

Hyperfine coupling constant	Transition at 1.53 mT	Type		263 K	280 K	296 K	311 K
A_1	3-4	π	w_1	0.60	0.55	0.50	0.55
	3-5	σ	w_2	1.30	1.35	1.45	1.55
	2-5	π	w_3	1.25	1.50	1.50	1.25
	3-6	π	w_4	1.25	1.50	1.50	1.25
	2-6	σ	w_5	0.95	1.05	0.95	1.05
	1-6	π	w_6	1.40	1.30	1.30	1.20
A_2	3-4	π	w_7	0.75	0.80	0.65	0.75
	3-5	σ	w_8	1.30	1.35	1.45	1.55
	2-5	π	w_9	1.25	1.50	1.50	1.25
	3-6	π	w_{10}	1.25	1.50	1.50	1.25
	2-6	σ	w_{11}	0.95	0.95	0.95	0.95
	1-6	π	w_{12}	0.95	1.05	0.95	1.05

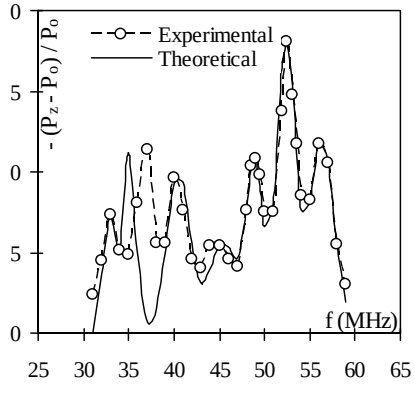

Fig. 6. Experimental points of the ESR spectra of the GALV/MBFA solution, the experimental fit function (20), and the theoretical fit function (21) for 263 K.

We have chosen two type complex formation with two different hyperfine coupling constants $A_1 = 12.01$ MHz and $A_2 = 8.92$ MHz of the nitrogen nucleus-free electron system. The energy diagrams of the spin system of the nitrogen spin 1 and the electron spin 1/2 for both A values was calculated from the Breit-Rabi formula, and is shown in Figure 2. All possible transitions at 1.53 mT were taken into account with the assumption that the experimental transition at 56.3 MHz is a 1-6 transition for A_1, and at 52.6 MHz a 1-6 transition for A_2. All π- and σ-type transition frequencies are given in Table 2. All transition frequencies obtained in the frequency interval 30 – 60 MHz for four temperatures are given in Table 3. The theoretical fit function is a sum of twelve Gaussians and is given by

$$y = \sum_{i=1}^{12} K_i \cdot \exp(-0.5 \cdot ((x - x_{ci})/w_i)^2), \qquad (21)$$

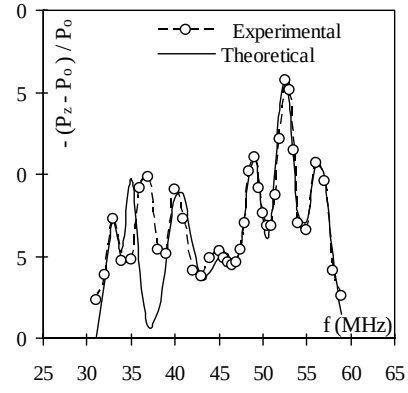

Fig. 7. Experimental points of the ESR spectra of the GALV/MBFA solution, the experimental fit function (20), and the theoretical fit function (21) for 280 K.

where $y = -(P_z - P_0)/P_0$ is the enhancement factor, the K_i's are the weight of the individual Gaussian which are tabulated in Table 4, the x_{ci}'s are the transition frequencies, and the w_i's are the standard deviation of the individual Gaussian which are tabulated in Table 5. The experimental points of the ESR spectra of the GALV/MBFA solution, the experimental fit function (20), and the theoretical fit function (21) for the temperatures 266 K, 280 K, 296 K, and 311 K are given in Figures 6 – 9. The R^2 values are 0.657, 0.663, 0.522, and 0.706, respectively, which point out the degree of agreement between the theoretical fit function (21) and the experimental values.

5. Conclusion

The present study reports experimental ESR spectra for some highly fluorinated aliphatic and aromatic solutions in a low magnetic field at different temperatures.

The coupled nuclear-electron systems exhibit two types of spin-spin interactions. These interactions are the dipolar interaction, which is proportional to the inverse cube of the distance between both spins of solvent nuclei and the unpaired electron of the free radical, and the scalar interaction, which is proportional to the unpaired electron density near the solvent nucleus.

The plane-plane collisions between GALV and OFT molecules cause dominantly a scalar coupling. Therefore, the details of the scalar (contact) interaction depend on the chemical and electronic properties of both interacting molecules.

We believe that in biological samples the detailed information of chemical environment could be obtained

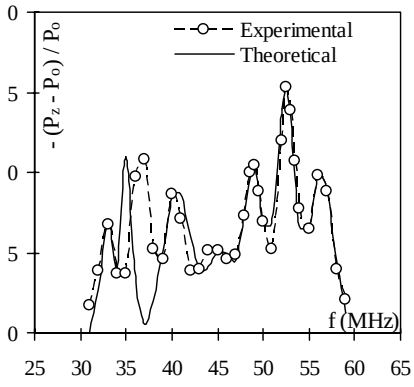

Fig. 8. Experimental points of the ESR spectra of the GALV/MBFA solution, the experimental fit function (20), and the theoretical fit function (21) for 296 K.

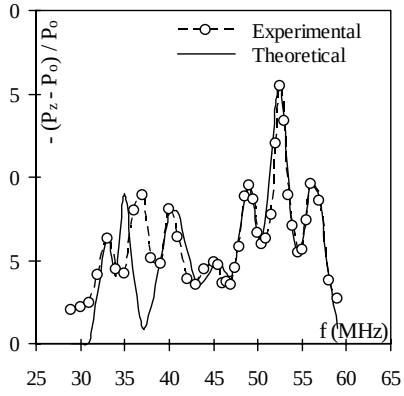

Fig. 9. Experimental points of the ESR spectra of the GALV/MBFA solution, the experimental fit function (20), and the theoretical fit function (21) for 311 K.

with aromatic fluorinated solvents and free radicals which are inclined to the scalar interaction in EPR oximetry supported by the Overhauser Effect [26, 27]. OFT may be a good oxygen tension reporter for biological samples due to its aromatic structure [28].

The high resolution ESR spectrum of the GALV/MBFA solution arises from the interaction of the unpaired electron, delocalized on the oxygen atom of GALV free radical molecule, and the nitrogen nucleus localized at the centre of the MBFA molecule. Probably the π-electron spin density increase at the nitrogen atom during the complex formation, resulting in a strong spin-spin interaction as if an intramolecular one.

We have chosen two type complex formation with two different spin-spin coupling parameters $A_1 = 12.01$ MHz and $A_2 = 8.92$ MHz. The energy diagrams of the spin system of the nitrogen spin 1 and the electron spin 1/2 for both A values was calculated from the Breit-Rabi formula. All possible transitions were taken into account and the experimental and theoretical fit parameters were determined.

The experimental points, the experimental fit function, and the theoretical fit function show that this is a new effect, which can be explained as an intramolecular spin-spin interaction.

Acknowledgements

This work was supported by Uludag University, Scientific Research Projects Unit grant no: 2009/44. The authors would like to thank the Uludag University for financial support and Prof. Dr. Emin N. Ozmutlu for his assistance in the preparation of the manuscript in English.

[1] A. W. Overhauser, Phys. Rev. **92**, 411 (1953).
[2] K. H. Hausser and D. Stehlik, Adv. Magn. Reson. **3**, 79 (1968).
[3] A. Yalçıner, Comm. Fac. Sci. Uni. Ankara, **27**, 1 (1978).
[4] W. Müller-Warmuth, Z. Naturforsch. **15a**, 927 (1960).
[5] M. M. Sünnetçioğlu, G. Bingöl, and R. Sungur, Z. Naturforsch. **46a**, 976 (1991).
[6] A. Oral Salman, M. M. Sünnetçioğlu, R. Sungur, and G. Bingöl, J. Magn. Reson. **134**, 1 (1998).
[7] I. Sert, M. M. Sünnetçioğlu, R. Sungur, and G. Bingöl, Z. Naturforsch. **55a**, 682 (2000).
[8] D. Grucker, T. Guiberteau, and B. Eclancher, Magn. Reson. Med. **34**, 219 (1995).
[9] D. Grucker, T. Guiberteau, B. Eclancher, J. Chambron, R. Chiarelli, A. Rassat, G. Subra, and B. Gallez, J. Magn. Reson. B **106**, 101 (1995).
[10] P. L. De Sousa, R. E. De Sousa, M. Engelsberg, and L. A. Colnago, J. Magn. Reson. **135**, 118 (1998).
[11] G. Planinšič, T. Guiberteau, and D. Grucker, J. Magn. Reson. B **110**, 205 (1996).
[12] R. B. Clarkson, B. M. Odintsov, P. J. Ceroke, J. H. Ardenkjaer-Larsen, M. Fruianu, and R. L. Belford, Phys. Med. Biol. **43**, 1907 (1998).
[13] A. Peksoz, M. A. Cimenoglu, and A. Yalciner, J. Disper. Sci. Technol. **29**, 40 (2008).
[14] A. Mülsch, D. J. Lurie, I. Seimenis, B. Fichtlscherer,

and M. A. Foster, Free Radical Bio. Med. **27**, 636 (1999).
[15] N. Nestle, K. Shet, and D. J. Lurie, Magn. Reson. Imag. **23**, 183 (2005).
[16] D. J. Lurie, G. R. Davies, M. A. Foster, and J. M. S. Hutchison, Magn. Reson. Imag. **23**, 175 (2005).
[17] A. L. Kleschyov, P. Wenzel, and T. Munzel, J. Chromatogr. B **851**, 12 (2007).
[18] E. H. Poindexter, J. Colloid Interface Sci. **38**, 412 (1972).
[19] A. Yalçıner, J. Colloid Interface Sci. **79**, 114 (1981).
[20] Z. Gülsün and A. Yalçıner, Commun. Fac. Sci. Univ. Ankara **29**, 1 (1980).
[21] K. D. Kramer and W. Müller-Warmuth, Z. Naturforsch. **19a**, 375 (1964).
[22] C. Akay and A. Yalçıner, Z. Naturforsch. **50a**, 177 (1995).
[23] M. A. Çimenoğlu, A. Kıvrak, and A. Yalçıner, in: Proceedings of the 13th Turkish Physics Conference, Eskişehir, 30. September 1992, p. 152.
[24] A. Yalciner, Dynamische Kernpolarisation und Substituenteneinflüsse auf Zwischenmolekulare Wechselwirkungen in Lösungen Freier Radikale. PhD thesis, Ankara University and Max-Planck Institute: Ankara, Turkey and Mainz, Germany 1970.
[25] K. Mukaı, M. Iızuka, and K. Ishızu, Bull. Chem. Soc. Jpn. **46**, 3578 (1973).
[26] T. Guiberteau and D. Grucker, J. Magn. Reson. **124**, 263 (1997).
[27] R. Murugesan, S. English, K. Reijnders, K. Yamada, J. A. Cook, J. B. Mitchell, S. Subramanian, and M. C. Krishna, Magn. Res. Med. **48**, 523 (2002).
[28] S. Hunjan, R. P. Mason, A. Constantinescu, P. Peschke, E. W. Hahn, and P. P. Antich, Int. J. Radiat. Oncol. Biol. Phys. **41**, 161 (1998).